Performance Improvements of Microchannel Heat Sink Using Wavy Channel and Nanofluids

Assel Sakanova, Chan Chun Keian, Jiyun Zhao*
EXQUISITUS, CENTRE FOR E-City, School of Electrical and Electronic Engineering, Nanyang Technological University, Singapore 639798
*Corresponding author: Tel.: +65-67904508, fax: +65-67933318, E-mail address: jyzhao@ntu.edu.sg

Abstract

To improve the heat transfer performances of microchannel heat sink (MCHS), the advanced channel structures and working fluids can be applied. In this paper, the wavy channel structure and application of nanofluids are investigated. The effects of wavy amplitude, wavelength, volumetric flow rate and volume fraction of different type of nanofluids are presented. Three wave amplitudes of 25 μm, 50 μm and 75 μm with two wavelength of 250 μm and 500 μm at volumetric flow rate ranges from 0.152 - 0.354 L/min are considered. Three different types of nanofluids with volume concentration ranges from 1% to 5% are applied. The effect of wavy MCHS is shown on thermal resistance, pressure drop, friction factor. It is found that in case of the pure water is applied as the coolant the heat transfer performance of the MCHS is significantly improved comparing with the traditional straight channel MCHS, while the replacement of the pure water by nanofluids makes the effect of wavy wall unnoticeable.

A	area (m^2)
c_p	specific heat (J/kg·K)
D_h	hydraulic diameter (m)
f	Fanning friction factor
h	heat transfer coefficient (W/Km^2)
h_{nf}/h_f	dimensionless heat transfer coefficient
H	height (m)
k	thermal conductivity (W/Km)
l	length (m)
N	number of micro-channels
Nu	Nusselt number
Δp	pressure drop (Pa)
P_{pump}	pumping power (W)
$\hat{P}$	dimensionless pressure
Pr	Prandtl number
q	heat flux (W/cm^2)
R_{th}	total thermal resistance (K/W)
Re	Reynolds number
t	thickness (m)
T	temperature (K)
U	velocity vector (m/s)
u, v, w	flow velocity (m/s)
W	width (m)
x, y, z	Cartesian coordinates

Greek symbols

α	aspect ratio
β	width ratio
δ	thickness of interfacial layer
η	fin efficiency
$k(\infty)$	Hagenbach factor
μ	viscosity ($N\cdot s/m^2$)
ρ	density (kg/m^3)
ϕ	viscous dissipation
φ	volumetric concentration of nanoparticles

Subscripts

app	apparent
av	average
ch	channel
eff	effective
f	fluid
j	junction
i	inlet
nf	nanofluid
o	outlet
s	solid

Keywords: CFD, micro-channel heat sink, wavy channel, nanofluids, heat transfer improvement

1. Introduction

With the recent development in computing technology over the past few decades, electronics have become smaller, faster and more powerful, which leads to an ever-increasing heat generation rate from electronics devices. To maintain the temperature of electronic components in safety zone, the chips are cooled by using forced air flow. However, standard cooling methods are not sufficient enough to deal with component that contains billions of transistors working at high frequency as the temperature can reach a critical level. Therefore

microscale cooling devices, such as microchannel heat sinks are important in heat removal applications in devices such as laser diode arrays and high-energy mirrors. In the past few decades, in order to meet the high heat dissipation rate requirements and maintain a low junction temperature, there are a lot of cooling technologies have been searched. After all the research have been done, the microchannel heat sink (MCHS) has attracted much attention due to the ability of producing high heat transfer coefficient, small size and volume per heat load, and small coolant requirements. Recent progress in the development of microchannel heat sinks was provided by Kandlikar et al [1].

A MCHS usually composed by a lot of parallel microchannels with a hydraulic diameter ranging from 10 to 1000 μm. A coolant flow through the micromachined or etched conduits with the purpose of removing heat from and generate uniform temperature distributions in micro-electro-mechanical systems, integrated circuit boards, laser-diode arrays, high-energy mirrors and other compact products with high transient thermal loads. The concept of MCHS cooling was first proposed by Tuckerman and Pease [2]. Since then, different kinds of materials were used by MCHS and channel dimensions have been investigated widely as well. These studies can be split into three categories, there are theoretical [3-4], numerical [5-8], and experimental approaches [9-10]. In the theoretical approach, the main purpose is to optimize MCHS performance by improving design structure. In this approach, most studies implemented the classical fin theory which models the solid walls separating microchannels as thin fins. The process of heat transfer process is summarizing as one dimensional, constant convection heat transfer coefficient and uniform fluid temperature. Nonetheless, the nature of the heat transfer process in MCHS is conjugated heat conduction in the solid wall and convection to the cooling fluid. The MCHS performance is inaccurate when the simplifications were used in theoretical approach. The simplifications used in the theoretical approach inaccurate MCHS performance.

Recently, the heat transfer and fluid flow processes in microchannel had been studied by Lee and Garimella [11] and detailed equations for designing microchannel geometries had been provided. After a while, another numerical and experimental investigation of heat transfer in rectangular microchannnels was performed by Lee and Garimella [12] whose width ranged from 194 mm to 534 mm. Based on the results, the conventional Navier-Stokes equations could be used to predict flow and heat transfer in the microchannels. Xie et al. [13, 14] investigate numerical studies on the laminar and turbulent flow and heat transfer characteristics of water-cooled straight microchannel heat sink. It showed that the removed heat flux increased from 256W/cm^2 to 350W/cm^2 with a nearly-optimized microchannel. Also, the pumping power increased from 0.205W to 5.365. W. Yin et al. [15] designed and optimized AlN – based MCHS for power electronics packaging. Sakanova et al. [16] optimised and compared three different structures of MCHS.

Wavy channel is an innovative concept to achieve higher heat transfer by modifying a plane straight channel and only cost of a slightly additional pressure drop. An experimental study regarding to wavy-walled channel to estimate heat and mass transfer for laminar and low Reynolds number flow was carried out by Goldstein and Sparrow [17]. It was found that the characteristic of heat transfer of the wavy channel was better than a parallel-plate channel within the Reynolds number range of 1000–1200. An experimental study of flow past a sinusoidal cavity by Saidi et al. [18] discovered that the heat and mass transfer properties were influenced by vortex evolution pattern, and that both pressure drop and heat transfer in the wavy channel were higher than those of a parallel-plate channel.

By using MCHS, high thermal performance can be achieved. However, further improvement is still essential to fulfil the demands from other device applications. Bergles and Webb [19-20] provided other reviews on the techniques for heat transfer enhancement in macroscale dimensions. Add additives to the working fluids are one of the methods to improve heat transfer. By adding additives, the fluid transport properties and flow features are changed which lead to enhance the heat transfer. In recent studies, metal particles implanted in the fluid were used to enhance the heat exchanger performance. However, there is a clogging issue occurred due to the particle sedimentation. By using this concept, the recent studied focused on enhancing heat transfer by using nanofluid in which nanoscale particles were suspended in the base fluids. Several experimental and analytical investigation showed that thermal conductivity are higher than pure fluids and therefore more efficient for cooling electronic devices [21-22].

In recent years, more studied focused on using a nanofluid as the heat transfer working fluid. There are two theoretical models were proposed by Xuan and Roetzel [23] to predict the heat transfer characteristics of nanofluid flow in a tube. Both convection heat transfer and pressure drop had been measured for nanofluid tube flows by Li and Xuan [24], Xuan and Li [25] and Pak and Cho [26]. Their results showed that the heat transfer coefficient could be greatly enhanced by modifying the flow Reynolds number, particle Peclet number, particle volume fraction, and particle size and shape. These studies also showed that there is no extra pressure drop after adding nanoparticle in the fluid. Lately, Yang et al. [27] implemented an experimental study regarding to

construct a heat transfer correlation based on the parameters that influenced heat transfer. For example, in a laminar flow in a circular tube, it showed that the heat transfer coefficient by using nanofluids working flow had a lower increase than predicted not only in the conventional heat transfer correlation for the homogeneous but also particle-suspended fluid. Several recent studies investigated the design of MCHS as well as double-layered MCHS with different geometric parameters by using nanofluids [28-31].

The flow characteristics of nanofluid heat transfer were carried out in macro-scale dimensions in most of the studies mentioned above. There are studies that analyzed the nanofluid flow and heat transfer in micro-scale dimensions [32-34]. In numerical aspect, different models of MCHS performance had been studied by Koo and Kleinstreuer and Jang and Choi [35-36] for the effective thermal conductivity of the nanofluids. In order to predict microchannel heat sink performance, a macro-scale correlation was carried out by Chein and Hunag [37]. In experimental aspect, Chein and Chuang [38] studied the behaviour of heat sink performance and effect of particle deposition when nanofluid is used as the working fluid. In the study of Lee and Mudawar [39], Al_2O_3–H_2O nanofluid was selected as working fluid. They discovered that the single-phase heat transfer coefficient can be enhanced by the high thermal conductivity of nanoparticles, especially for the laminar flow. As the complicated heat transfer phenomena and large variety in nanofluids, it is still essential to focused on investigating heat transfer characteristics in micro-scale dimensions and nanofluid flow.

In this study 3D heat transfer of wavy MCHS is investigated and compared with rectangular MCHS. The effect of water as well as nanofluids as a coolant in both types of MCHS is discussed. The effects of the wave amplitude, wavelength, flow rate and the volume concentration of three types of nanofluids on the heat transfer, pressure drop, friction factor and thermal resistance are discussed and compared with rectangular MCHS.

2. Computational model

2.1 Straight Microchannel Heat Sink

There are total 71 period of microchannels are arranged in a substrate in this study. The geometric dimensions of MCHS are taken from optimally designed MCHS [40] and shown in Table 1. The optimally design parameters are obtained by using a novel inverse problem solution method of a simplified conjugate-gradient method and a full three-dimensional heat transfer and flow model. Under constant area, heat flux and pump power, three design parameters such as number of channels, channel aspect ratio and channel width ratio is optimized in order to achieve the minimum thermal resistance. The bottom size is 28mm*100mm and the heat flux with 100W/cm^2 is received from the bottom surface (Fig. 1a). Due to the structure of the microchannel heat sink is periodic in this study, one of the microchannel is taken as the computational domain. In this model, both the two sides of the microchannel contain a half-wall. The geometry parameters of each microchannel are as follows: wall thickness $W_r/2$= 28μm; channel width W_c = 85μm; channel height H_c= 700 μm; and cover plate thickness H_r= 100 μm. The rectangular straight microchannel heat sink is used as the baseline microchannel heat sink.

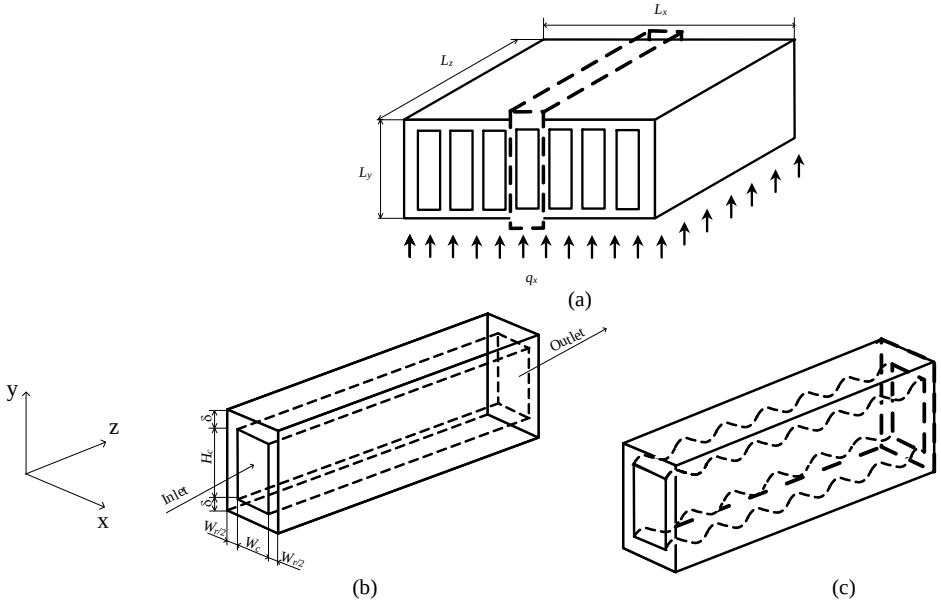

Fig. 1: Schematic of microchannel heat sink, (a) heat sink, (b) straight microchannel (c) wavy channel

L_z (mm)	L_y (mm)	L_x (mm)	W_c (μm)	W_r (μm)	H_c (μm)	q (W/cm^2)
10	900	10	85	56	700	100

Table 1. Optimal geometric dimensions [40]

The improvement of the wavy microchannel on thermal performance and pressure drop therefore can be evaluated by comparing the results of different heat sink model.

2.2 Single-Layer Wavy Microchannel Heat Sink

In this study, single layer wavy microchannel heat sink is a further improvement of model from rectangular straight microchannel, as shown in Fig. 1(c). Therefore, all of the dimensions are same as the rectangular straight microchannel. The only change is the direction of the fluid flow is in wave form with a sine curve expressed by the trigonometric function, as below.

$$y = A\sin\left(2\pi \cdot \frac{z}{\lambda}\right) \tag{1}$$

The waviness, γ, is defined as follows.

$$\gamma = \frac{A}{\lambda} \tag{2}$$

where A and λ are defined as amplitude and wavelength, respectively. Also, z is defined as the flow direction. Three wave amplitudes of 25 μm, 50 μm and 75 μm are considered in this study. And λ is selected as 0.5mm (500 μm) and 0.25mm (250 μm), therefore there are in total 20 periods and 40 periods of waves in the computational model accordingly. The total length in z direction therefore is 0.01 m (1cm). Furthermore, same as the rectangular straight microchannel, only one branch of the wavy microchannels was selected as the computational model to reduce the time consumption.

2.3 Assumption

To simplify the analysis in this project, there are several assumptions made regarding the operating conditions of a wavy channel MCHS.

1. The fluids maintain in conditions such as single phase, incompressible laminar flow across a channel.
2. Both thermally and hydraulically fully developed flow (steady-state conditions)
3. Gravitational force is negligible and radiation heat transfer exists.
4. The thermophysical properties of the solid are polynomial (temperature dependent).
5. The surface of the MCHS is well insulated.

2.4 Governing equations and boundary conditions

Based on the assumptions above, the governing equations for this model are as follows.

Continuity equation for the coolant:

$$\frac{\partial u}{\partial x} + \frac{\partial v}{\partial y} + \frac{\partial w}{\partial z} = 0 \tag{3}$$

where u, v, and w are defined as the velocity components in the x, y, and z directions, respectively.

Momentum equations for the coolant:

$$\rho_f\left(u\frac{\partial u}{\partial x} + v\frac{\partial u}{\partial y} + w\frac{\partial w}{\partial z}\right) = -\frac{\partial P}{\partial x} + \mu_f\left(\frac{\partial^2 u}{\partial x^2} + \frac{\partial^2 u}{\partial y^2} + \frac{\partial^2 u}{\partial z^2}\right) \tag{4}$$

$$\rho_f\left(u\frac{\partial v}{\partial x} + v\frac{\partial v}{\partial y} + w\frac{\partial v}{\partial z}\right) = -\frac{\partial P}{\partial y} + \mu_f\left(\frac{\partial^2 v}{\partial x^2} + \frac{\partial^2 v}{\partial y^2} + \frac{\partial^2 v}{\partial z^2}\right) \tag{5}$$

$$\rho_f\left(u\frac{\partial w}{\partial x} + v\frac{\partial w}{\partial y} + w\frac{\partial w}{\partial z}\right) = -\frac{\partial P}{\partial z} + \mu_f\left(\frac{\partial^2 w}{\partial x^2} + \frac{\partial^2 w}{\partial y^2} + \frac{\partial^2 w}{\partial z^2}\right) \tag{6}$$

Where ρ_f and μ_f are the density and dynamic viscosity of the coolant, respectively, and p is the coolant pressure.

Energy equation for the coolant:

$$\rho_f c_{p.f}\left(u\frac{\partial T_f}{\partial x}+v\frac{\partial T_f}{\partial y}+w\frac{\partial T_f}{\partial z}\right)=k_f\left(\frac{\partial^2 T_f}{\partial x^2}+\frac{\partial^2 T_f}{\partial y^2}+\frac{\partial^2 T_f}{\partial z^2}\right) \tag{7}$$

Energy equation for the solid region

$$0=k_s\left(\frac{\partial^2 T_s}{\partial x^2}+\frac{\partial^2 T_s}{\partial y^2}+\frac{\partial^2 T_s}{\partial z^2}\right) \tag{8}$$

In this study, liquid water is used as the baseline working fluid to evaluate the improvement of the nanofluids. For water, the temperature dependent density is given by Thiesen-Scheel-Diesselhorst equation [41]. Dependence of dynamic viscosity on temperature is defined by Sherman [42]. Expressions for specific heat capacity and thermal conductivity are obtained by third-order polynomial fitting results of data [43]. The expressions of temperature dependent thermo physical properties are given by

$$\rho(T)=1000\left[1-\frac{T+15.9414}{508929.2(T-204.87037)}(T-276.9863)^2\right] \tag{9}$$

$$\mu(T)=1.005\times10^{-3}\left(\frac{T}{293}\right)^{8.9}\exp\left[4700\left(T^{-1}-293^{-1}\right)\right] \tag{10}$$

$$c_p(T)=3908+3.826T-0.01674T^2+2.330\times10^{-5}T^3 \tag{11}$$

$$k_f(T)=-1.579+0.01544T-3.515\times10^{-5}T^2+2.678\times10^{-8}T^3 \tag{12}$$

The temperature-dependent thermal properties of liquid water are replaced by nanofluids, which are also temperature-dependent. The effective density, heat capacity, dynamic viscosity and thermal conductivity of nanofluids have the following forms [44-48]:

Density:

$$\rho_{nf}=(1-\varphi)\rho_f+\varphi\rho_p \tag{13}$$

Heat capacity:

$$c_{p,nf}=\frac{\varphi\rho_p c_{pp}+(1-\varphi)\rho_f c_{pf}}{\rho_{nf}} \tag{14}$$

Dynamic viscosity:

$$\frac{\mu_{nf}}{\mu_f(T)}=123\varphi^2+7.3\varphi+1 \tag{15}$$

Thermal conductivity:

According to the correlation of Xuan and Roetzel [49], the thermal conductivity of a nanofluid can be written as

$$k_{nf}=k_o+C^*\rho_{nf}c_{p,nf}\varphi(H_c/2)u \tag{16}$$

where k_o represents the stagnant effective thermal conductivity of the nanofluid. C* is an empirical constant, and u_m is the mean velocity of the nanofluid along the z direction. The stagnant thermal conductivity k_o can be calculated from Xie et al. [50] as

$$k_o=\left(1+3\theta\varphi_T+\frac{3\theta^2\varphi_T^2}{1-\theta\varphi_T}\right)k_f \tag{17}$$

with

$$\theta=\frac{\beta_{1f}\left[(1+\gamma)^3-\beta_{p1}/\beta_{f1}\right]}{(1+\gamma)^3+2\beta_{1f}\beta_{p1}} \tag{18}$$

$$\varphi_T=\varphi(1+\gamma)^3 \tag{19}$$

$$\gamma=\delta/\mathrm{d}_p \tag{20}$$

$$\beta_{1f} = \frac{k_1 - k_f}{k_1 + 2k_f} \tag{21}$$

$$\beta_{p1} = \frac{k_p - k_1}{k_p + 2k_1} \tag{22}$$

$$\beta_{f1} = \frac{k_f - k_1}{k_f + 2k_1} \tag{23}$$

$$k_1 = \frac{k_f M^2}{(M - \delta / d_p)\ln(1+M) + M\delta / d_p} \tag{24}$$

$$M = k_p / k_f (1 + \delta / d_p) - 1 \tag{25}$$

Here, φ_T, δ, d_p, and r_p represent the effective particle volume fraction, thickness of the interfacial layer, and particle diameter, respectively.

The velocity inlet is defined with uniform temperature of 298 K while velocity inlet is specified as 0.6 m/s, 0.8 m/s, 1 m/s, 1.2 m/s, 1.4 m/s which corresponds to Reynolds number ranges from 99-232 and volumetric flow rate 0.152 L/min, 0.203 L/min, 0.253 L/min, 0.304 L/min, 0.354 L/min accordingly. The pressure outlet is adopted with atmosphere pressure. Constant heat flux 100 W/cm^2 is specified at the bottom of MCHS. Symmetrical boundary conditions are assumed on the left and right sides. Therefore, the boundary conditions are listed as below.

The associated boundary conditions for the governing equations are given at the following:

Inlet

$$u = u_{in},\ v = 0,\ w = 0,\ T = T_{in} \tag{26}$$

Outlet

$$p = p_{out} \tag{27}$$

Coolant – solid interface:

$$u = 0,\ \ v = 0,\ w = 0,\ T = T_{in} \tag{28}$$

Bottom wall of the heat sink:

$$q_w = -k_s \frac{\partial T_s}{\partial n} \tag{29}$$

Other solid walls and symmetric boundaries:

$$-k_s \frac{\partial T_s}{\partial n} = 0 \tag{30}$$

Reynolds number is defined as

$$\mathrm{Re} = \frac{\rho u_{av} D_h}{\mu} \tag{31}$$

where D_h is the hydraulic diameter and defined as $D_h = 2H_{ch}W_{ch}/(H_{ch}+W_{ch})$.

In order to investigate the influence of nanofluid in MCHS, the total thermal resistance of MCHS is given by

$$R_{th} = \frac{T_j - T_{in}}{qA} \tag{32}$$

where T_j is the junction temperature, T_{in} is the inlet temperature of coolant, qA is the heat flow.

The average Nusselt number is calculated by

$$Nu_{av} = \frac{h_{av} D_h}{k_{f,av}} \tag{33}$$

average heat coefficient which is defined by

$$h_{av} = \frac{k_{f,av} Nu}{D_h} \tag{34}$$

The pumping power is given by

$$P_{pump} = \Delta p \cdot \dot{V} \tag{35}$$

where Δp is the pressure drop of working liquid between inlet and outlet, V is the volumetric flow rate of working liquid with the expression $V = NAu_{av}$.

The dimensionless Fanning friction factor is defined as

$$f = \frac{D_h \Delta p}{2\rho_{av} u_{av}^2 L_x} \tag{36}$$

3. Numerical method

3.1 Mesh size sensitivity

Based on ANSYS Fluent, the 3D conjugate heat transfer problem is numerically solved. Implicit solver option is used to solve the governing equations. The second order upwind scheme is adopted for both energy and momentum discretization. And for pressure discretization, standard interpolation scheme is adopted. The pressure-velocity coupling is implemented by SIMPLE algorithm. The convergence criteria for the *x*, *y*, and *z* directions velocity is 10^{-6} while the residuals of energy equations are restricted to 10^{-7}. There are 3 types of quadrilateral meshes with grid lines of 120×41×34, 140×78×41 and 240×78×41 are investigated. The impact of mesh density on the simulation results are shown in Fig. 2. The difference of maximum temperatures is 0.017% between 120×41×34 and 140×78×41, while 0.0178% between 120×41×34 and 240×78×41. With respect to pressure drop distribution, the maximum deviation occurs at the end of the channel with 0.0125% between 120×41×34 and 140×78×41 and 0.7% between 120×41×34 and 240×78×41. Finally, 120×41×34 grid was selected as the best trade-off between both accuracy and CPU time. By using mesh grid with 120×41×34, based on the periodic conditions and symmetry, the time consume can be reduced and get the same result at the same time, as shown in Fig. 2, computational time and grid size are reduced. The fine boundary layer grid is chosen since it retains a high amount of accuracy as shown in Fig. 3.

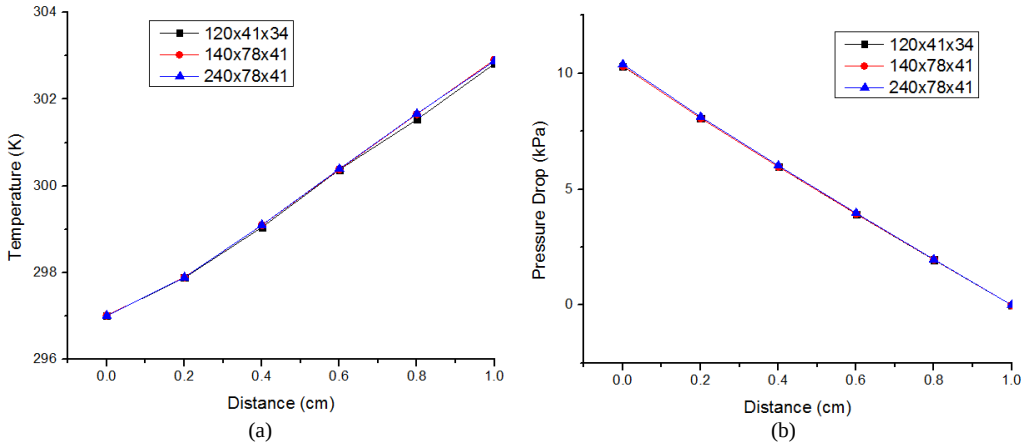

(a) (b)

Fig. 2. Comparison of streamwise temperature distribution (a) and pressure drop distribution (b) with various mesh density

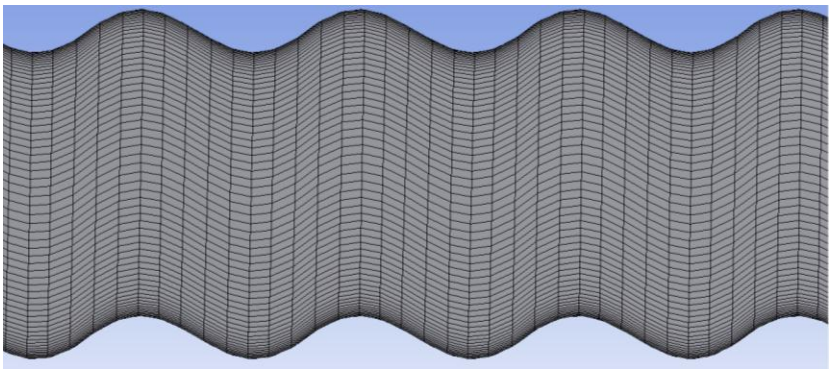

Fig. 3. Fine boundary layer grid

3.2 Experimental validation

To verify the model accuracy the simulation results have been benchmarked with experimental work [2]. Table 1 shows the data of both experimental and simulation results. The discrepancies are 5%, 7% and 14% for cases №1, 2 and 3 respectively.

No.	$w_{ch}(\mu m)$	$w_w(\mu m)$	$H_c(\mu m)$	P (psi)	q (W/cm^2)	R_{th} ($^oC/W$)	
						Experimental data [1]	Simulation data
1	56	44	320	15	181	0.110	0.104
2	55	45	287	17	277	0.113	0.105
3	50	50	302	31	790	0.090	0.077

Table 2. The geometric parameters of experimental work and thermal resistance of experimental and simulation results

4. Results and discussions

4.1 Effect of wavy amplitude and wavelength

In order to investigate the effect of wavy wall of MCHS, water has been firstly used as a coolant. Fig. 4 shows the thermal resistance and pressure drop versus volumetric flow rate for both rectangular and all wavy microchannel heat sink.

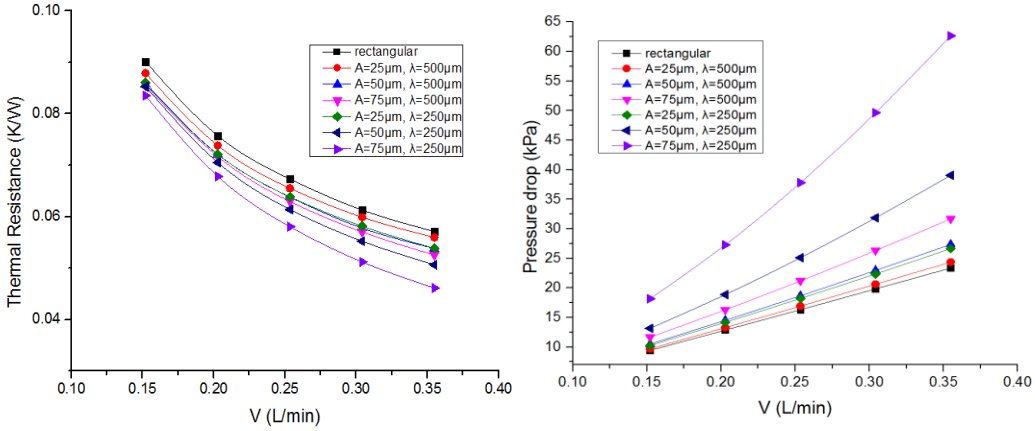

(a) (b)

Fig. 4. Relation between (a) thermal resistance (b) pressure drop and volumetric flow rate in rectangular channel and wavy channel

From Fig. 4(a), it shows that the relation of thermal resistance and volumetric flow rates are inversely proportional. As the volumetric flow rates increases, thermal resistance decreases. It can be seen that the minimum thermal resistance in this cases is A=75μm with λ=250μm. Also, it is obvious that the thermal resistance of rectangular channel is higher than all wavy cases. A significant improvement of heat transfer performance can be found in the comparison between wavy channel and rectangular channel.

From Fig. 4(b), it can be observed that the relation between pressure drop and volumetric flow rates are proportional. As the volumetric flow rate increases, pressure drop increases as well. It is apparent that wavy channel has higher pressure drop compare to rectangular channel. Furthermore, the higher the amplitude of

wavy channel, the higher pressure drop received. For example, the case of A=75µm with λ=250µm contain the highest pressure drop among all the cases, which is also about 1.38 times compare to rectangular channel for low Reynolds number and it becomes 1.45 times with high Reynolds number. Also, it is apparent that the same amplitude with shorter wavelength of wavy channel has a higher pressure drop compare to longer wavelength. The pumping power required is proportional to pressure drop so as to support enough power to fluid to overcome the friction. Therefore it can be concluded that wavy channel with λ=250µm consume more pumping power than λ=500µm.

Fig. 5 shows that the velocity vector of rectangular channel and wavy channel along z-axis with various amplitude with Reynolds number of 99. No vertical structure can be observed in wavy channel due to low Reynolds number and the microscale size of the channels. It can be observed that the flow is a fully developed parabolic Poiseuille flow type, dominated by viscous forces. Due to Dean number is lower compare to critical Dean number, Dean vortices therefore cannot be developed. Also, no vortices are inspected in this type of flow [51]. The maximum velocity in z direction is shifted from the centerline to the wavy peaks due to wavy structure, and it accelerates the flow next to wavy peaks. The hydrodynamic and thermal boundary layers are therefore getting thinner. Thus, there is an increment in heat transfer coefficient. Furthermore, the heat transfer coefficient also increases by increasing the wavy amplitude and Reynolds number. Along with this reason, the increment of surface area results in a small heat transfer improvement.

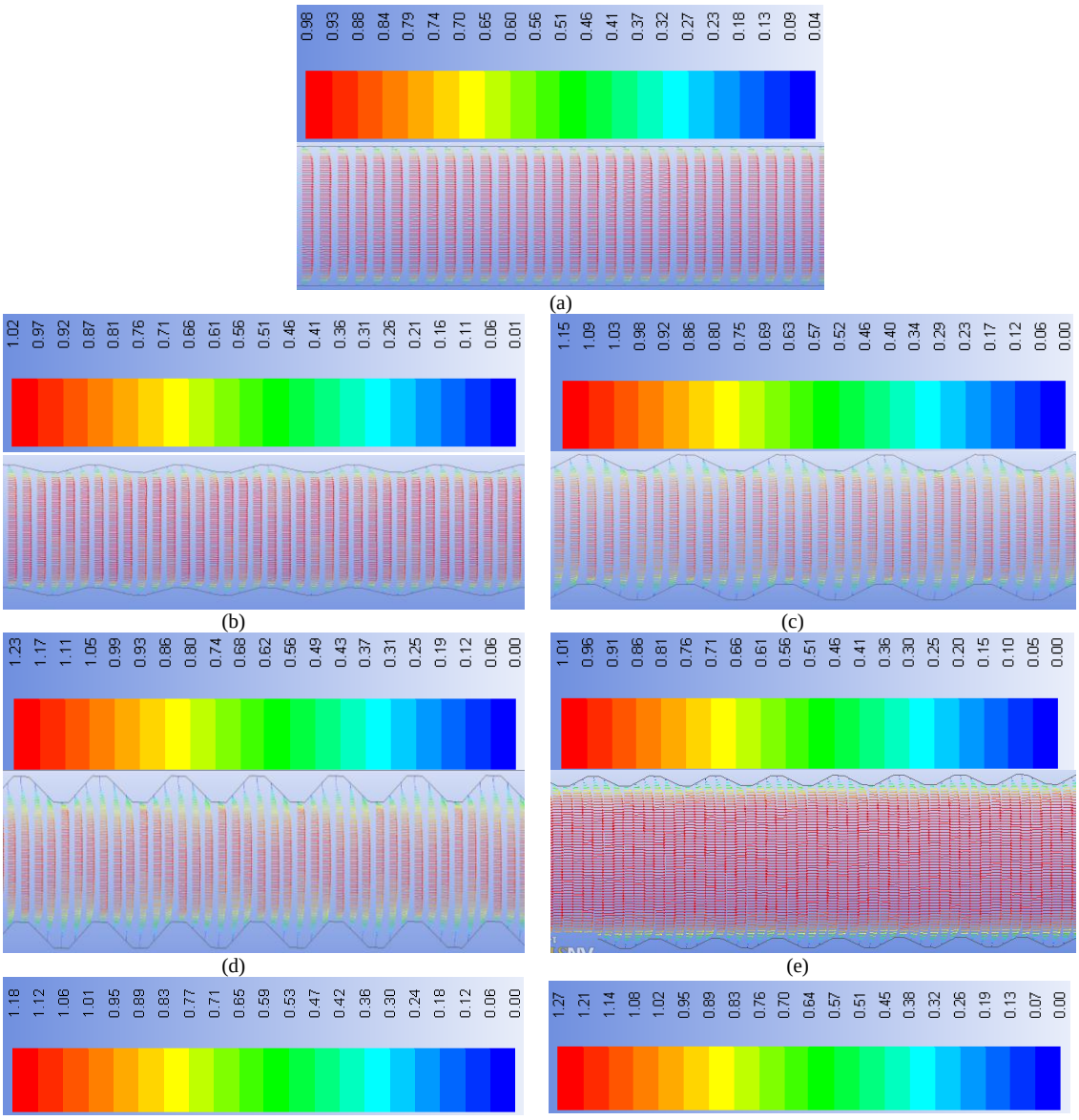

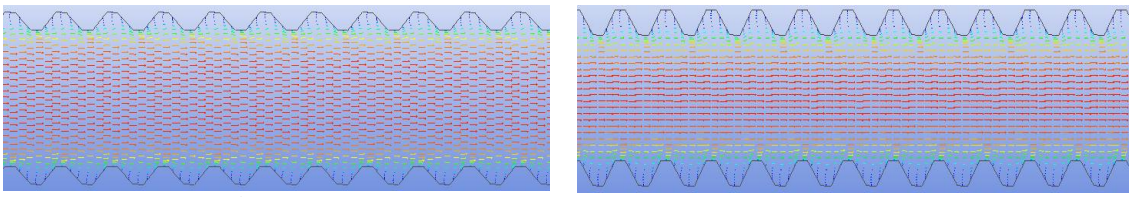

(f) (g)

Fig. 5. Vectors of velocity of wavy channel along z-axis with different amplitude - A (a) A=0µm (straight), (b) A=25µm and λ=500µm, (c) A=50µmand λ=500µm, (d) A=75µmand λ=500µm, (e) A=25µm and λ=250µm, (f)A=50µm and λ=250µm,(g) A=75µm and λ=250µm

Fig. 6 shows the velocity profile of rectangular and wavy channels. The maximum velocity of the parabolic velocity profile in rectangular channel can be found in the centre of the channel. It can be observed that the maximum velocity shifted from centre to the side. Also, it can be seen from Fig. 6(b) that even up to Reynolds number of 232, there is no boundary layer separation by observing the effect of wavelength. Same theory of decreasing wavelength can be applied to explain the effect of increasing wave amplitude. The decrement of wavelength lead to the thermal boundary layers and hydrodynamic thinner because of the maximum velocity of the geometry governed biased shift from the channel centre to the troughs and crests. Similar results can be found in [52].

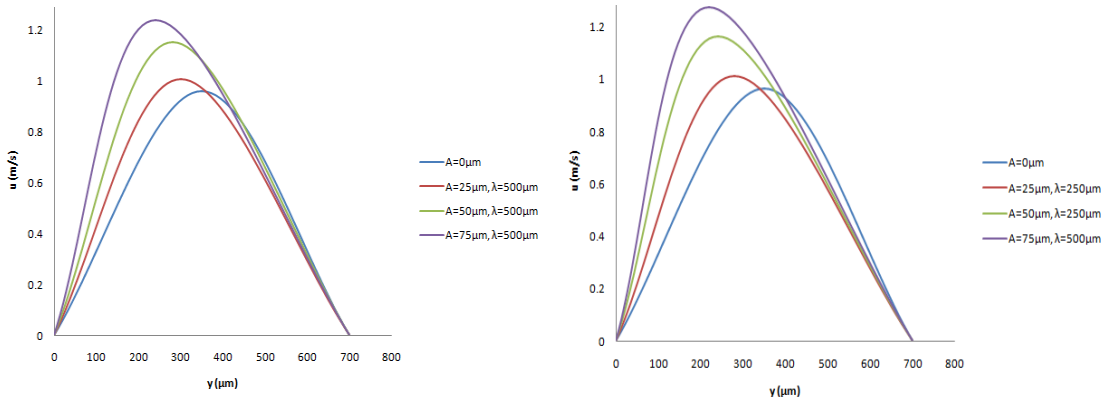

(a) (b)

Fig. 6. Velocity profile of rectangular channel and wavy channel with different (a) amplitude (b) wavelength

Fig. 7(a) shows the heat transfer coefficient of ratio in rectangular channel and wavy channel with different cases. It can be estimated that there is an improvement of heat transfer to all wavy channel compare to straight channel. Also, it can be seen that there is no significant improvement in case of A=25µm and λ=500µm compare to rectangular channel as the heat transfer coefficients are close to each other. It can also be observed that A=75µm and λ=250µm performed the best heat transfer performance compared to other cases, followed by A=50µm and λ=250µm, A=75µm and λ=500µm, A=50µm and λ=500µm, A=25µm and λ=250µm and A=25µm and λ=500µm. From Fig. 7(a) it can be seen that the decrement of wavelength has better effect compare to the increment of amplitude. Also, from Fig. 7(b), it is shows that the temperature increase in almost a linear form as the inlet velocity reduced along the channel.

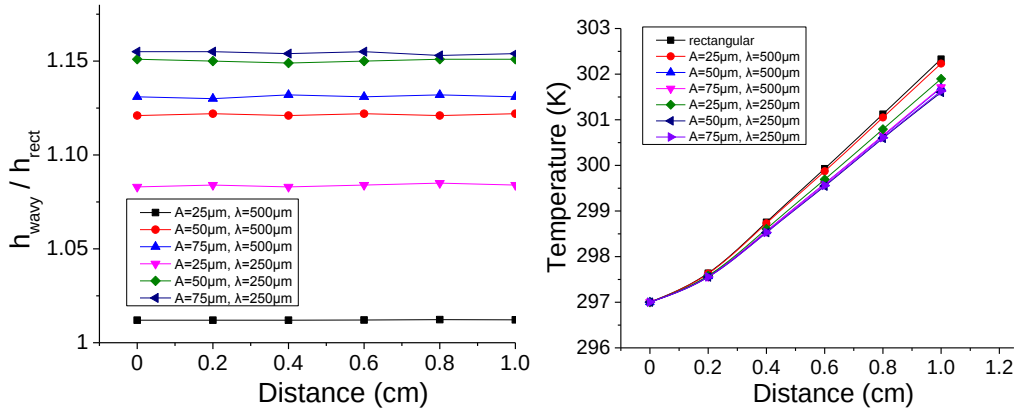

(a) (b)

Fig. 7. Dimensionless local heat transfer coefficient ration of rectangular channel to wavy channel (a) along the channel length (b) temperature distribution along the channel length for all cases

4.2 Nanofluids effect in wavy MCHS

Fig. 8 depicts the effect of using nanofluids in wavy channel as coolant with different amplitude and wavelength. It can be seen in Fig. 8 that the thermal resistance of wavy channel with diamond nanofluid as well as water as a coolant decreases almost linearly when the Reynolds number increases. Also, as the nanoparticle volume fraction increases, the thermal resistances decrease even further.

However, the effect of nanofluids reduces when wavy amplitude increases and wavelength decreases. 1% and 5% of nanofluid volume concentration is used as an example to observe this phenomenon in these studies. Tables 3, 4 show the improvement in thermal resistance when diamond (1%, 5%) - water nanofluid is used as a comparison with pure water, low and high Reynolds numbers are selected.

Volume concentration of nanoparticle	Reynolds number	Amplitude (μm)	Wavelength (μm)	Improvement in thermal resistance
1%	Low	25	500	10.86%
		50		10.71%
		75		10.51%
		25	250	10.44%
		50		9.98%
		75		8.52%
	High	25	500	24.1%
		50		22.93%
		75		21%
		25	250	21.78%
		50		18.73%
		75		14.89%

Table 3. Comparison of thermal resistance between nanofluid and pure water

Volume concentration of nanoparticle	Reynolds number	Amplitude (μm)	Wavelength (μm)	Improvement in thermal resistance
5%	Low	25	500	6.83%
		50		6.63%
		75		6.06%
		25	250	5.8%
		50		5.5%
		75		5.34%
	High	25	500	10.23%
		50		10.06%
		75		9.67%
		25	250	9.4%
		50		9.15
		75		8.92%

Table 4. Comparison of thermal resistance between nanofluid-5% and nanofluid-1%

Based on the results, it shows that the effect of 2-5% of volume concentration of diamond nanofluid in wavy channel is close to each other. Furthermore, it can be observed that as the percentage of volume concentration increases, the less improvement of heat transfer performance can be provided by increasing wavy amplitude and decreasing wavelength.

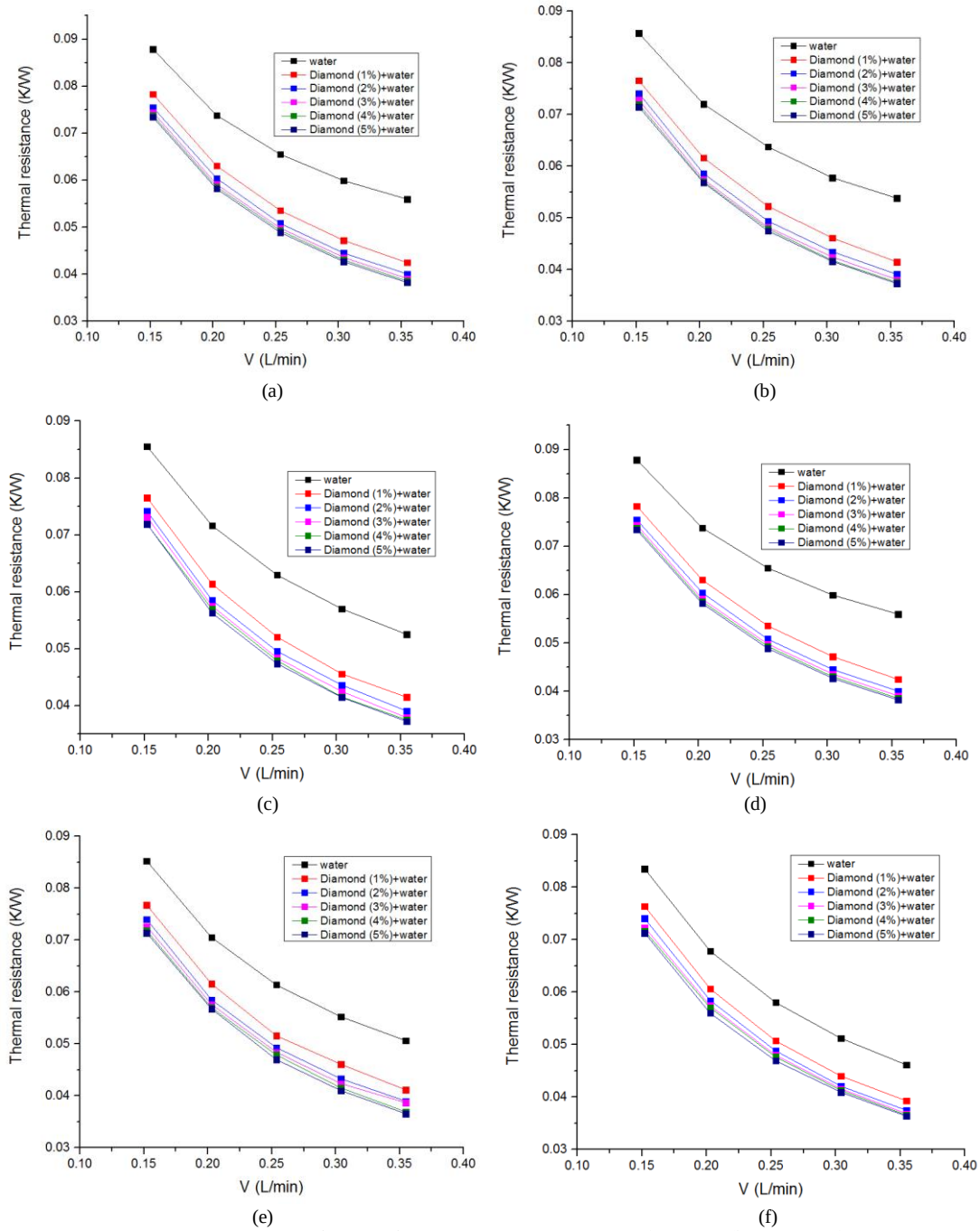

Fig. 8. Thermal resistance versus volumetric flow rate for wavy channel: (a) A=25μm, λ=500μm (b) A=50μm, λ=500μm (c) A=75μm, λ=500μm (d) A=25μm, λ=250μm (e) A=50μm, λ=250μm (f) A=75μm, λ=250μm

This phenomenon can be defined due to the value of thermal boundary layer thickness is higher for nanofluid than that of pure fluid. According to reference [53], thermal boundary layer is defined as

$$\delta_t \cong \delta / \mathrm{Pr}^{1/3} \tag{17}$$

where δ is defined as the hydrodynamic boundary layer over a flat plate, which is function of Reynolds number and it can be calculated by

$$\delta = 5x / \sqrt{\mathrm{Re}_x} \tag{18}$$

where x is a position along the plate

Also, the boundary layer ration of pure fluid to that of the nanofluid is given by

$$\frac{\delta_{t,f}}{\delta_{t,nf}} = \sqrt{\frac{\mu_f}{\mu_{nf}}} \cdot \sqrt{\frac{\rho_{nf}}{\rho_f}} \cdot \frac{\mathrm{Pr}_{nf}^{1/3}}{\mathrm{Pr}_f^{1/3}} \tag{19}$$

where Pr is Prandtl number, it can be calculated by using $Pr = c_p\mu/k_f$. Also, δ_t is thermal boundary layer of pure water and $\delta_{t,nf}$ is thermal boundary layer of nanofluid.

The Fig. 9 shows the ratio of boundary layer of water to that of the nanofluid for volume concentration of diamond-water nanofluid ranged from 1% to 5%. It can be seen that $\delta_t/\delta_{t,nf}<1$ for $\phi>0$ and $\delta_t/\delta_{t,nf}=1$ for $\phi=0$. Same results are obtained in [54].

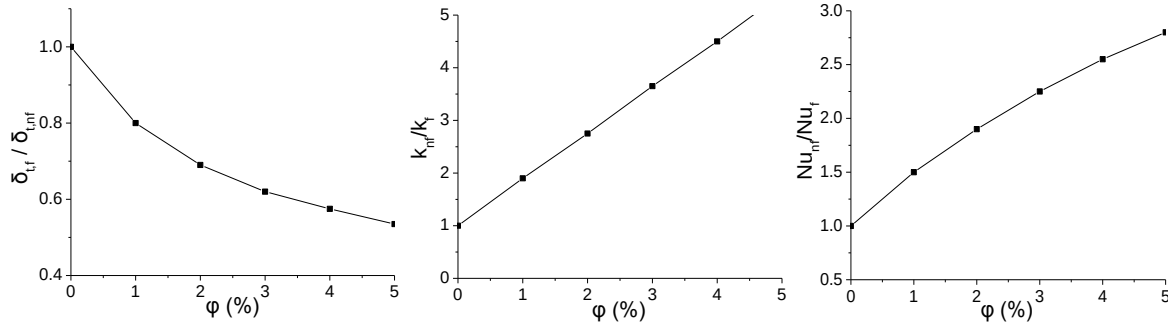

(a) (b) (c)

Fig. 9. The thermal boundary layer ratio of (a) pure water to diamond (1%) - water nanofluid, (b) the thermal conductivity ratio of diamond (1%) - water nanofluid to pure water and (c) the Nu number ratio of diamond (1%) - water nanofluid to the pure water (u=0.6m/s)

Fig. 10 shows the dimensionless average heat transfer coefficient against Re in wavy channels. The range of volume concentration of nanofluid is from 1% to 5%. The results show that the dimensionless average heat transfer coefficient increases when Reynolds number increase. At the same time, the boundary layer decreases and temperature gradients in boundary layer increases as well. Both advantages and disadvantages can be observed by increasing the volume concentration of nanofluid. The advantage is the thermal conductivity increases when the volume concentration of nanofluid increases. On the other hand, Fig. 9 shows that thermal boundary layer is enlarged due to the increment of volume concentration of nanofluid. The net effect on the average Nusselt number increases as the volume concentration of nanofluid increases as shown in Fig. 9(c). Although this effect of nanofluid volume concentration in Fig. 9 is defined for flat plate, similar phenomenon is expected for wavy channels. The same results and expected trends is obtained in [54].

Fig. 10 also shows that the explanation of nanofluid effect mentioned above is also applicable for the wavy channel. It can be observed that as volume concentration nanofluid increases, dimensionless average heat transfer increases as well. Also, for higher Re, there is a noticeable improvement in overall performance compare to lower Re. Also, it can be observed that the improvement due to nanofluids decreases as the amplitude of wavy channel increase and wavelength decreases. All these result indicates that the influence of wavy channel to the decrement of thermal boundary layer thickness for nanofluid is lesser than water. Also, the shift of the maximum velocity from the centerline to the wavy peaks is less noticeable and it farther less noticeable with increase in volume concentration of nanofluid. It means the effect of higher amplitude as well as shorter wave length resulting in a small overall improvement while major enhancement is owing to enhance the thermal conductivity which increases with volume concentration of nanofluids. For wavy channel the increase in volume concentration of nanofluid provides the same improvement in thermal conductivity as for rectangular channel while the decrease in thermal boundary layer is comparably lower for that of wavy channel. It explains why the highest impact of nanofluid belongs to the rectangular channel rather than for any wave channel cases.

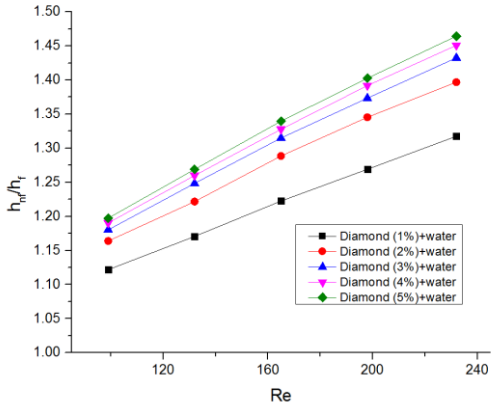
h_{nf}/h_f
Re
Diamond (1%)+water
Diamond (2%)+water
Diamond (3%)+water
Diamond (4%)+water
Diamond (5%)+water

(a)

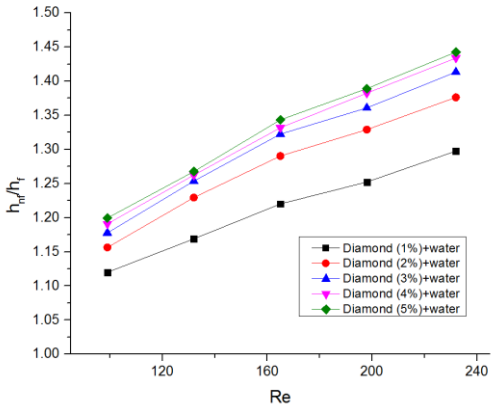
h_{nf}/h_f
Re
Diamond (1%)+water
Diamond (2%)+water
Diamond (3%)+water
Diamond (4%)+water
Diamond (5%)+water

(b)

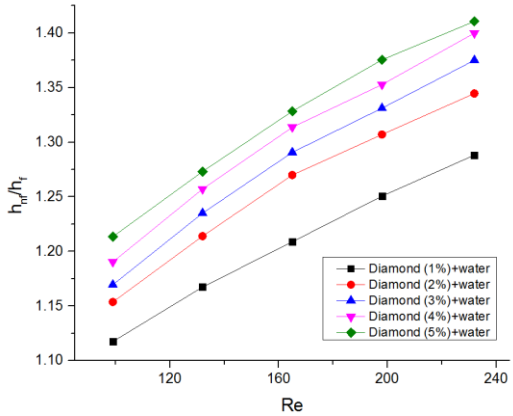
h_{nf}/h_f
Re
Diamond (1%)+water
Diamond (2%)+water
Diamond (3%)+water
Diamond (4%)+water
Diamond (5%)+water

(c)

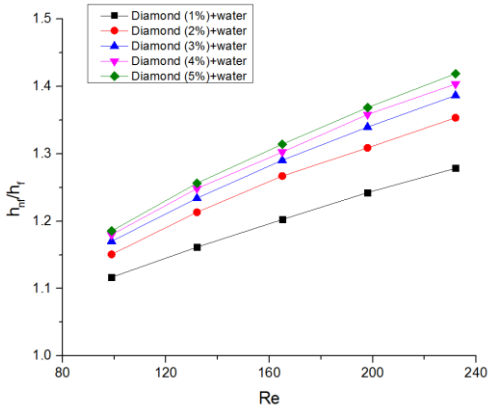
h_{nf}/h_f
Re
Diamond (1%)+water
Diamond (2%)+water
Diamond (3%)+water
Diamond (4%)+water
Diamond (5%)+water

(d)

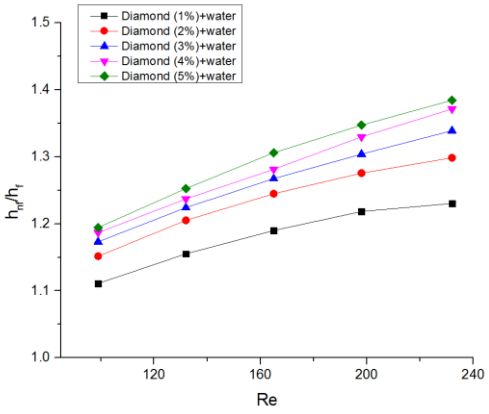
h_{nf}/h_f
Re
Diamond (1%)+water
Diamond (2%)+water
Diamond (3%)+water
Diamond (4%)+water
Diamond (5%)+water

(e)

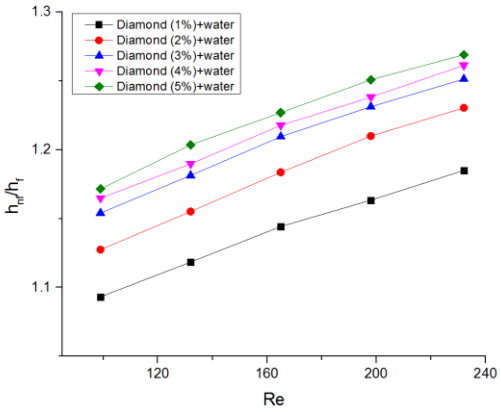
h_{nf}/h_f
Re
Diamond (1%)+water
Diamond (2%)+water
Diamond (3%)+water
Diamond (4%)+water
Diamond (5%)+water

(f)

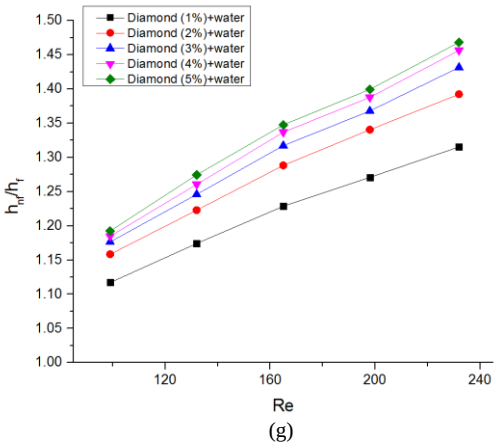

Fig. 10. Dimensionless average heat transfer coefficient versus Reynolds number at different diamond - water nanofluid volume concentration for the cases when (a) A=25µm and λ=500µm, (b) A=50µm and λ=500µm, (c) A=75µm and λ=500µm , (d) A=25µm and λ=250µm, (e) A=50µm and λ=250µm, (f) A=75µm and λ=250µm and (g) rectangular channel

The higher volume concentration of nanofluids the lower the decrement in thermal boundary layer due to wavy geometry. It becomes the reason of an imperceptible effect of wavy structure for higher volume fraction of nanofluids as illustrated in Fig. 11.

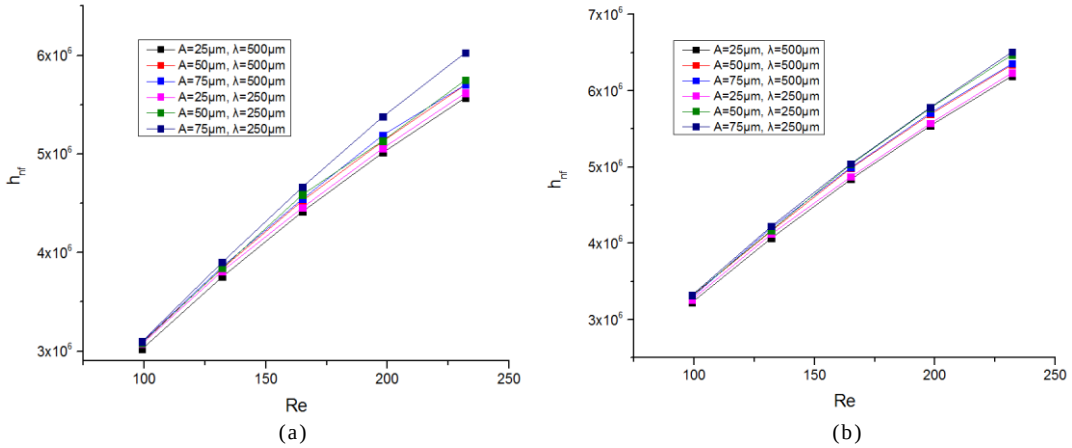

Fig. 11. Heat transfer coefficients dependence on Re with (a) diamond (1%) – water nanofluid and (b) diamond (5%) – water nanofluid

4.3 Effect of nanoparticle type in wavy channel

So far there is no studied regarding to applying different types of nanofluid in wavy channel heat sink. Therefore, the 3D heat transfer of wavy channels is investigated numerically by using various types of nanofluids such as diamond-water, CuO-water, and SiO_2 – water nanofluids. The range of volume concentration is from 1% to 5% of nanoparticle and the range of Reynolds number is from 99 to 232. Table 5 below shows the thermo-physical properties of nanoparticles.

Property	**Nanoparticle**		
	Diamond (Al_2O_3)	CuO	SiO_2
Density, ρ (kg/m^3)	3510	6500	2200
Thermal conductivity, k (W/mK)	1000	20	1.2
Specific heat capacity, c_p (J/kgK)	497.26	535.6	703

Table 5. Thermal-physical properties of nanofluids

The UDF file of temperature-dependent thermo physical properties of nanofluids is created based on equations (13-16). Fig. 12 shows the result of the temperature distribution along the centerline of the heated wall. Water as well as various types of nanofluid with 1% volume concentration and the case of A=25µm and

λ=500µm is selected. It can be observed that water has the highest temperature compare to other types of nanofluids. Also, nanofluids show the same trend as water for increasing temperature along the length of channel. In this case, diamond has the lowest temperature followed by SiO_2, and CuO. It has the same order of nanofluid performance with [55].

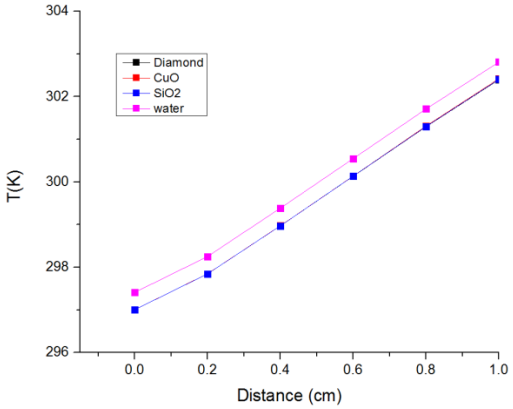

Fig. 12. The temperature distribution along the centre line of the heated wall and various types of fluids are used as coolant

The case A=25µm and λ=500µm at high and low Reynolds number is selected to investigate the effect of the nanoparticle volume concentration on the overall thermal resistance. Based on the result from Fig. 13, as the volume concentration of nanofluid increases, the overall thermal resistance decreases. Also, the highest improvement of thermal resistance can be observed at 1% of volume concentration of nanofluid. It can be observed that diamond provided the lowest thermal resistance compare to other types of nanofluids. The effect of nanofluids can be explained as follows. The presence of nanoparticle in base fluids increases both thermal conductivity and dynamic viscosity follow by reduction in heat capacity. By increasing thermal conductivity, convective heat transfer coefficient can be enhanced as well. At the same time, there is an increment in dynamic viscosity and reduction in heat capacity which causes the reduction of mean velocity of nanofluids. Therefore the less improvement of the convection heat transfer as predicted by [53, 56].

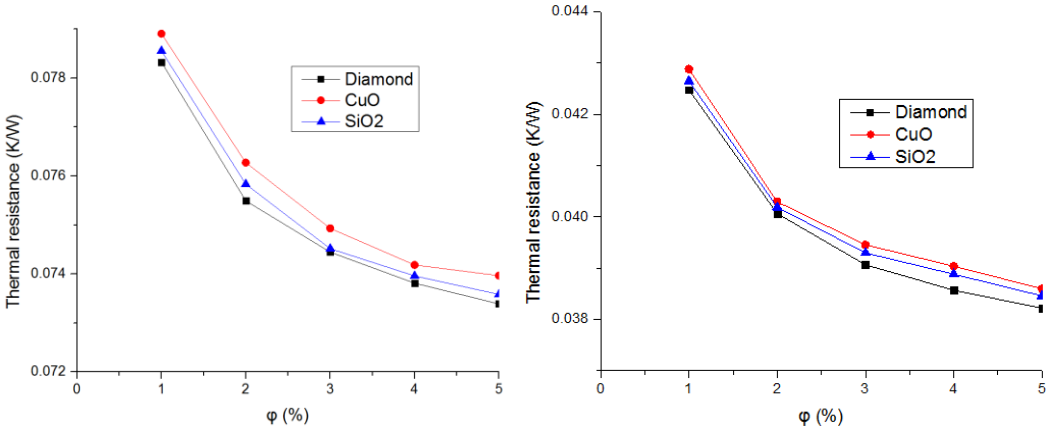

Fig. 13. Overall thermal resistance versus volume concentration of various types of nanofluid (a) Re= 99 (b) Re= 232

Fig. 14 shows the results of dimensionless pressure drop along the channel length for different types of fluid. Cases of volume concentration of nanofluid with 1% and 5% at Reynold number with 99 and 232 with A=25µm and λ=500µm are selected. It is apparent that the highest pressure can be seen at the entrance of the channel and it decrease along the channel. It is because high pressure is required to push the coolant. Also, all the coolant reaches the atmosphere pressure at the outlet therefore no significant different can be found. By observing the inlet of the channel, it shows that nanofluids provide higher pressure drop compare to water. In terms of nanofluid, CuO – water nanofluid has the lowest value of pressure drop followed by diamond and SiO_2 – water nanofluid. This order of nanofluid performance in wavy MCHS coincides with triangular microchannels [53]. Also, larger differences of pressure drop between water and nanofluid can be found by increasing both Reynold number and volume concentration of nanofluid. However the sequence of nanofluid

performance is the same as for rectangular MCHS. It implies that wavy geometry does not change the consistency of nanofluid implementation while the larger pressure drop is needed due to increment in wavy amplitude and reduction in wavelength.

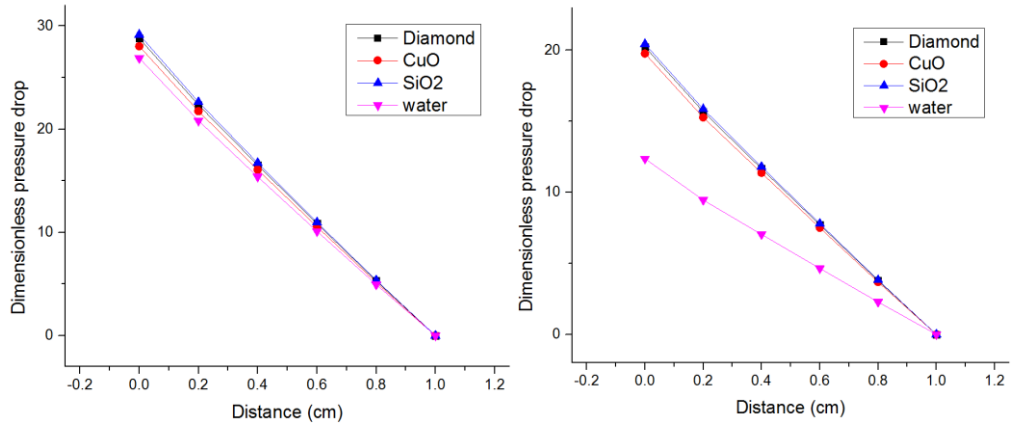

(a) (b)

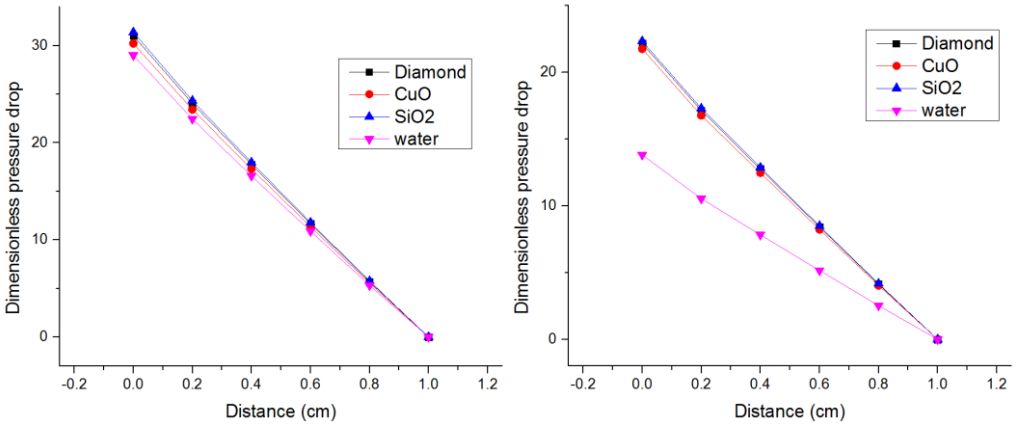

(d) (e)

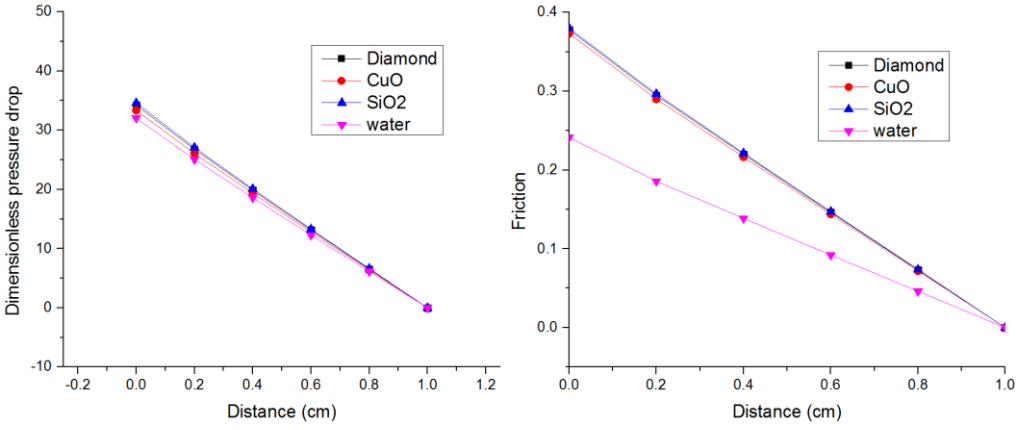

(f) (g)

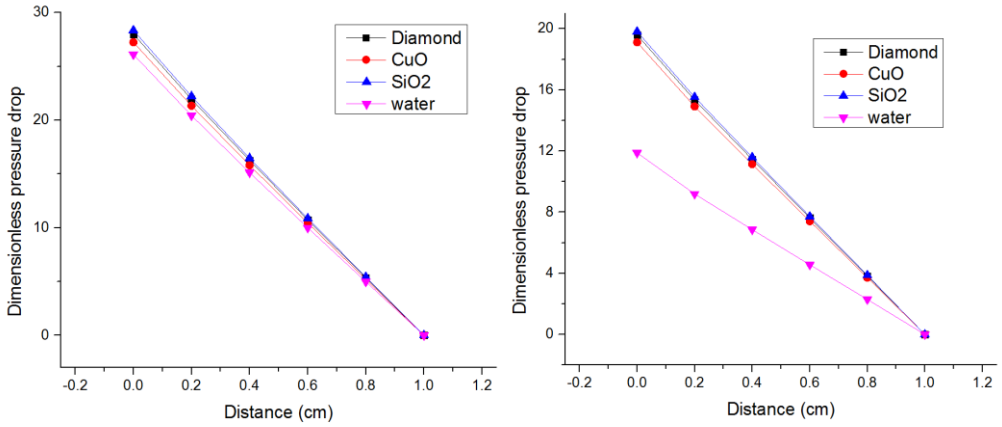

Fig. 14. Dimensionless pressure drop along the channel length for water and different types of nanofluid with 1% (Fig. a, c, e) and 5% of volume concentration (Fig. b, d, f) at Re = 99 (Fig. a, c, e, g) and Re = 232 (Fig. b, d, f, h) for the cases when A=25μm and λ=500μm(a, b) A=50μm and λ=500μm (c, d)A=75μm and λ=500μm and (g, h) rectangular channel.

Fig. 15 shows the effect of friction factor for various types of nanofluid in wavy channel at Reynold number 232. It can be seen that the friction factor decreases along the channel length for all cases due to the reduction in pressure drop. The friction factor is higher for nanofluids and it increases with enlargement in wavy amplitude and decrease in wavelength.

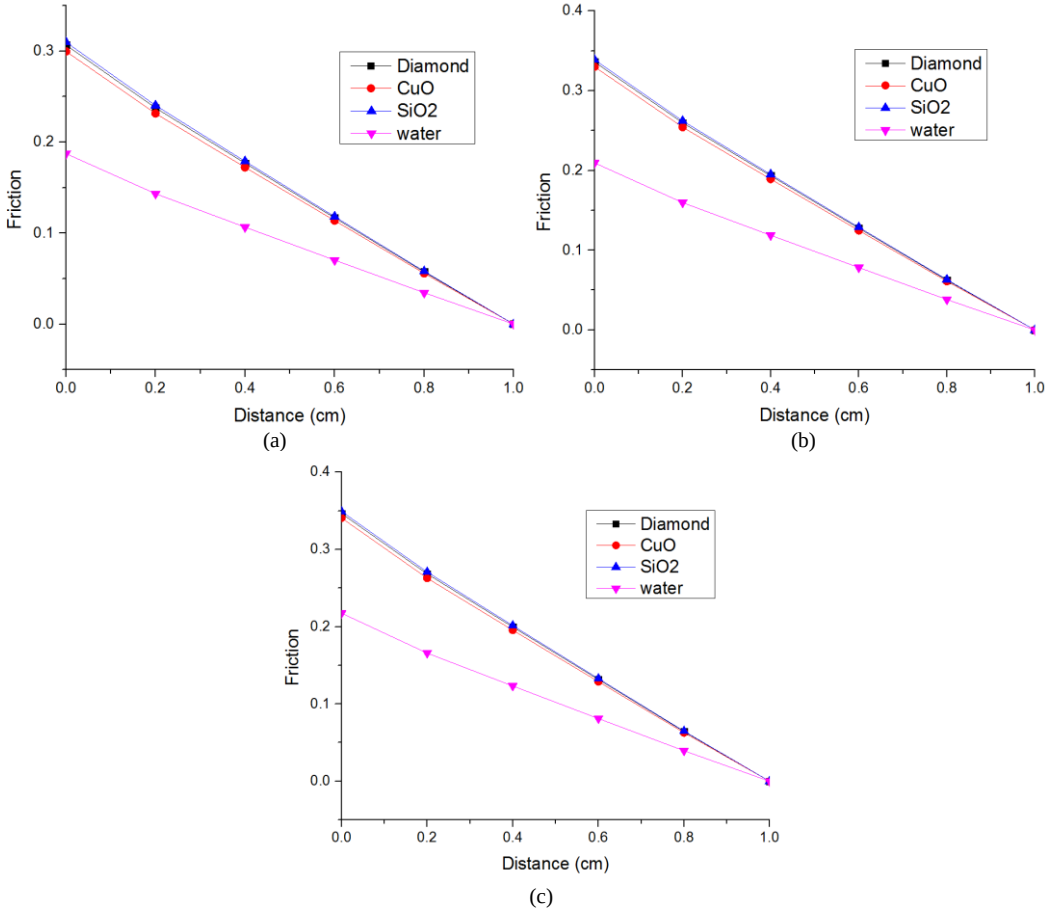

Fig. 15. Friction factor of wavy channel along the channel length for various nanofluids with Reynold number 232 at cases of (a) A=25μm and λ=500μm (b) A=50μm and λ=500μm (c) A=75μm and λ=500μm

4.4 Comparison of rectangular channel with water and wavy channel with nanofluid

Since diamond nanoparticle dispersed in water yields the best heat transfer improvement and it further increases with volume concentration, we compared the cooling performance of rectangular MCHS applying pure water and diamond (5%) – water nanofluid with wavy MCHS applying diamond (5%) – water nanofluid as presented in Fig. 16. According to the Fig. 16(a) there is no apparent difference in thermal resistance among wavy channel cases and rectangular channel with diamond (5%) – water nanofluid. All of these cases are able to enhance the thermal performance by the same value. However pressure drop increases with higher amplitude and shorter wavelength. This implies that wavy geometry has less noticeable effect if nanofluids are applied as a coolant.

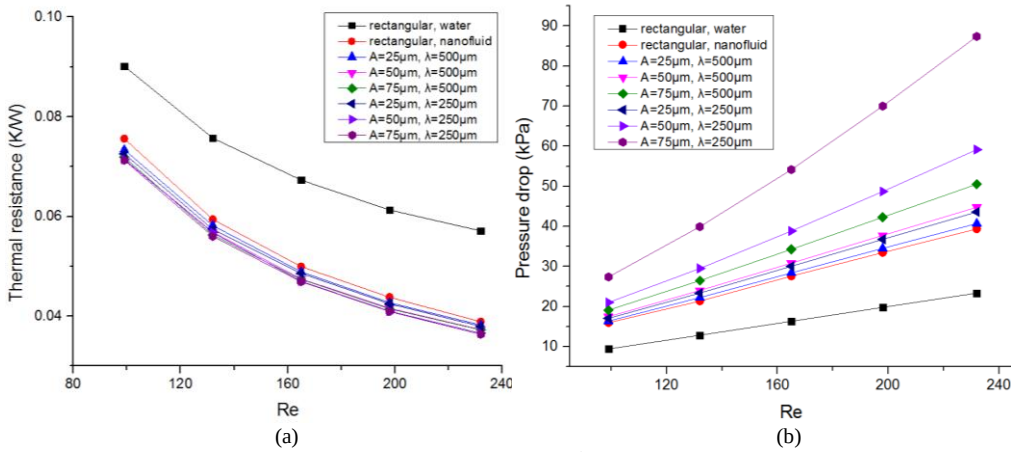

(a) (b)

Fig. 16. (a) Thermal resistance (b) and pressure drop dependence on Re for rectangular MCHS using pure water and wavy MCHS usingdiamond (5%) – water nanofluid as the coolant.

5. Conclusions

Heat transfer in a 3D wavy microchannel heat sink using three various types of nanofluids with temperature-dependent thermophysical properties is investigated by a numerical study. The effects of wavy amplitude, wavelength, volumetric flow rate and volume fraction of different type of nanofluids are investigated.

In a case when water is applied as a coolant, the wavy MCHS overcomes cooling performance of traditional rectangular MCHS. Moreover the higher the amplitude and shorter the wavelength of wavy channel, the less thermal resistance. And the overall improvement due to wavy channels is more noticeable at high Re as compare to at low Re. The positive effect of wavy geometry is owing to the thinning of the thermal and hydrodynamic boundary layer. However, the increase in amplitude and decrease in wavelength provides additional pressure drop.

In a case when nanofluids is applied as a coolant, it makes the effect of wavy channels imperceptible and wavy as well as rectangular MCHS yields the very similar cooling performance.

The performance of three types of nanofluids has been investigated in this study. All of them show better cooling implementation as compare to pure water. However, the presence of nanofluids results in an increase in pressure drop and friction factor. Diamond – water nanofluid exhibits the best performance by providing the highest heat transfer coefficient and the lowest thermal resistance among other nanofluids. Moreover wavy geometry does not change the consistency of nanofluids implementation which is the same as for rectangular channel.

References

1. S.G. Kandlikar, W.J Grande, Evolution of microchannel flow passages – thermohydraulic performance and fabrication technology, Heat Transfer Eng. 24 (2003) 3–17.
2. D.B. Tuckerman, R.F. Pease, High performance heat sinking for VLAI, IEEE Electron. Devices Lett. EDL-2 (1981) 126-129.
3. R.W Knight, D.J. Hall, J.S. Goodling, R.C. Jaeger, Heat sink optimization with application to microchannels. IEEE Trans on Compon., Hybrids, and Manuf. Technol. 15 (1992) 832–842.
4. K.K. Ambatipudi, M.M. Rahman, Analysis of conjugate heat transfer in microchannel heat sinks, Numer. Heat Transfer Part A 37 (2000) 711–731.

5. A.G. Fedorov, R. Viskanta, Three-dimensional conjugate heat transfer in the microchannel heat sink for electronic packaging. Int. J. Heat and Mass Transfer 43 (2000) 399–415.
6. P. Lee, S.V. Garimella, D. Liu, Investigation of heat transfer in rectangular microchannels, Int. J. Heat and Mass Transfer 48 (2005) 1688–1704.
7. J. Li, G.P. Peterson, P. Cheng, Three-dimensional analysis of heat transfer in a micro-heat sink with single phase flow, Int. J. Heat and Mass Transfer 47 (2004) 4215–4231.
8. J. Li, G.P. Peterson, Geometric optimization of a micro heat sink with liquid flow. IEEE Trans. Compon. Packag. Technol. 29 (2006) 145–154.
9. W. Qu, I. Mudawar, Experimental and numerical study of pressure drop and heat transfer in a single-phase microchannel heat sink. Int. J. Heat and Mass Transfer 45 (2002) 2549–2565.
10. I. Tiselj, G. Hetsroni, B. Mavko, A. Mosyak, E. Pogrebnyak, Z. Segal, Effect of axial conduction on the heat transfer in microchannels. Int. J. Heat and Mass Transfer 47 (2004) 2551–2565.
11. P. S. Lee, S. V. Garimella, and D. Liu, Investigation of heat transfer in rectangular microchannels, Int. J. Heat and Mass Transfer 48 (2005) 1688–1704.
12. P. S. Lee and S. V. Garimella, Thermally developing flow and heat transfer in rectangular microchannels, Int. J. Heat Mass Transfer 49 (2006) 3060–3067.
13. X. L. Xie, Z. J. Liu, Y. L. He, and W. Q. Tao, Numerical study of laminar heat transfer and pressure drop characteristics in a water-cooled minichannel heat sink, Appl. Therm. Eng, 29 (2009) 64–74.
14. X. L. Xie, W. Q. Tao, and Y. L. He, Numerical study of turbulent heat transfer and pressure drop characteristics in a water-cooled minichannel heat sink, ASME J. Electron. Packag. 129 (2007) 247–255.
15. S. Yin, K,J, Tseng, J. Zhao, Design of AlN-based micro-channel heat sink in direct bond copper for power electronics packaging, Appl. Therm. Eng. 52 (2013) 120-129.
16. A. Sakanova, S. Yin, J. Zhao, J. M. Wu, K.C. Leong, Optimization and comparison of double-layer and double-side micro-channel heat sinks with nanofluid for power electronics cooling, Appl. Therm. Eng. 65 (2014) 124-134
17. J. L. Goldstein and E. M. Sparrow, Heat and mass transfer characteristics for flow in a corrugated wall channel, ASME J. Heat Transfer 99 (1977) 187–195.
18. C. Saidi, F. Legay, and B. P. Fotch, Laminar fow past a sinusoidal cavity, Int. J. Heat Mass Transfer 30 (1987) 649–660.
19. A.E. Bergles, ExHFT for fourth generation heat transfer technology, Exp. Therm. Fluid Sci. 26 (2002) 335–344.
20. R.L. Webb, Principles of Enhanced Heat Transfer. John Wiley & Sons, New York 1993.
21. X. Wang, X. Xu, S.U.S. Choi, Thermal conductivity of nanoparticle– fluid mixture. J. of Thermophysics and Heat Transfer 13 (1999), 474–480.
22. J. Koo, C. Kleinstreuer, A new thermal conductivity model for nanofluids. Journal of Nanoparticle Research 6 (2004) 577–588.
23. Y. Xuan, W. Roetzel, Conceptions for heat transfer correlation of nanofluids. Int. J. Heat and Mass Transfer 43 (2000) 3701– 3707.
24. Q. Li, Y. Xuan, Convective heat transfer and flow characteristics of Cu–water nanofluid. Science in China E 45 (2002) 408–416.
25. Y. Xuan, Q. Li, Investigation on convective heat transfer and flow features of nanofluids. ASME Journal of Heat Transfer 125 (2003) 151–155.
26. B.C. Pak, Y.L. Cho, Hydrodynamic and heat transfer study of dispersed fluids with submicron metallic oxide particles, Experiment. Heat Transfer 11 (1998) 151–170.
27. Y. Yang, Z. Zhang, E.A. Grulke, W.B. Anderson, Heat transfer properties of nanoparticle influid dispersions (nanofluids) in laminar flow, Int. J. Heat Mass Transfer 48 (2005) 1107–1116.
28. T. C. Hung, W.M. Yan, X.D. Wang, C.Y. Chang, Heat transfer enhancement in microchannel heat sinks using nanofluids, Int. J. Heat Mass Transfer 55 (2012) 2559-2570
29. T. C. Hung, W.M. Yan and W.P. Li, Analysis of heat transfer characteristics of double-layered microchannel heat sink, Int. J. Heat Mass Transfer 55 (2012) 3090-3099
30. T. C. Hung and W.M. Yan, Enhancement of thermal performance in double-layered microchannel heat sink with nanofluids, Int. J. Heat Mass Transfer 55 (2012) 3225-3238
31. J. C. Ho, W.C. Chen and W.M. Yan, Correlations of heat transfer effectiveness in a minichannel heat sink with water-based suspensions of Al_2O_3 nanoparticles and/or MEPCM particles, Int. J. Heat Mass Transfer 69 (2014) 276-284

32. X. D. Wang, B. An, L. Lin, J.L. Xu, Optimal geometric structure for nanofluid-cooled microchannel heat sink under various constraint conditions, Energy Convers and Manage 65 (2013) 528-538
33. X. D. Wang, B. An, L. Lin, D.J. Lee, Inverse geometric optimization for geometry of nanofluid-cooled microchannel heat sink, Appl. Therm. Eng. 55 (2013) 87-94
34. L. Lin, Y.Y. Chen, X.X. Zhang, X.D. Wang, Optimization of geometry and flow distribution for double- layer microchannel heat sink, Int. J. of Therml Sci. 78 (2014) 158-168
35. J. Koo, C. Kleinstreuer, Laminar nanofluid flow in microheatsinks. Int. J. of Heat and Mass Transfer 48 (2005), 2652–2661.
36. S.P. Jang, S.U.S. Choi, Cooling performance of a microchannel heat sink with nanofluids. Appl. Therm. Eng. 26 (2006), 2457–2463.
37. R. Chein, G. Hunag, Analysis of microchannel heat sink performance using nanofluids. Appl. Therm. Eng. 25 (2005) 3104–3114.
38. R. Chein, J. Chuang, Experimental microchannel heat sink performance studies using nanofluids, Int. J. of Therml Sci. 46 (2007), 57–66.
39. J. Lee, I. Mudawar, Assessment of the effectiveness of nanofluids for single-phase and two-phase heat transfer in micro-channels. Int. J. Heat and Mass Transfer (2006)
40. Z. H. Wang, X. D. Wang, W.M. Yan, Y.Y. Duan, D. J. Lee, Multi-parameters optimization for microchannel heat sink using inverse problem method, Int. J. Heat Mass Transfer 43 (2011) 3701-3707.
41. S.C. McCutcheon, J.L. Martin and T.O. Barnwell, Jr., Handbook of Hydrology, McGraw-Hill, New York, 1993
42. F.C. Sherman, Viscous Flow, McGraw-Hill, New York, 1990.
43. T.L. Bergman, A.S. Lavine, F.P. Incropera, D.P. Dewitt, Fundamentals of heat and mass transfer, 7th edition, John Willey & Sons, 2011
44. Y. Xuan, W. Roetzel, Conceptions for heat transfer correlation of nanofluids, Int. J. Heat Mass Transfer 43 (2000) 3701–3707.
45. H.C. Brinkman, The viscosity of concentrated suspensions and solutions, J. Chem. Phys. 20 (1952) 571–581.
46. M. Hosseini, S. Ghader, A model for temperature and particle volume fraction effect on nanofluid viscosity, J. Mol. Liq. 153 (2010) 139–145.
47. S.E.B. Maiga, C.T. Nguyen, N. Galanisb, G. Roy, Heat transfer behaviours of nanofluids in a uniformly heated tube, Superlattices Microstruct. 35 (2004) 543–557.
48. I.M. Krieger, T.J. Dougherty, A mechanism for non Newtonian flow in suspensions of rigid spheres, Trans. Soc. Rheol. 3 (1959) 137–152.
49. Y. Xuan, W. Roetzel, Conceptions for heat transfer correlation of nanofluids, Int. J. Heat Mass Transfer 43 (2000) 3701–3707.
50. H. Xie, M. Fujii, X. Zhang, Effect of interfacial nano-layer in the effective thermal conductivity of nano-particle fluid mixture, Int. J. Heat Mass Transfer 48 (2005) 2926-2932
51. H. Y. Zhang, D. Pinjala, T. N. Wong, K.C. Toh and Y. K. Joshi, Single-phase liquid cooled microchannel heat sink for electronic packages, Appl. Therm. Eng. 25 (2005), 1472-1487.
52. G. Xie, Z. Chen, B. Sunden, W. Zhang, Numerical predictions of the flow and thermal performance of water-cooled single-layer and double –layer wavy microchannel heat sinks, Numerical Heat Transfer, Part A, 63: 201-225, 2013
53. F.P Incropera, D.P. Dewitt, T. L. Bergman, A.S. Lavine, Fundamentals of Heat and Mass Transfer, sixth ed, John Wiley & Sons, 2007, pp. 405-409
54. H. Heidary, M. J Kermani, Effect of nano-particle on forced convection in sinusoidal-wall channel, Int. Commun. Heat Mass Transfer 37 (2010) 1520-1527
55. H. A. Mohammed, P. Gunnasegaran, N. H. Shuaib, The impact of various nanofluid types on triangular microchannels heat sink cooling performance, Int. Commun. Heat Mass Transfer 38 (2011) 767-773.
56. C. J. Ho, L.C. Wei, Z.W. Li, An experimental investigation of forced convection cooling performance of a microchannel heat sink with Al_2O_3/water nanofluid, Appl. Therm. Eng. 30 (2010) 96-103